IEEE Access
Multidisciplinary | Rapid Review | Open Access Journal

Received August 24, 2021, accepted September 5, 2021, date of publication September 13, 2021,
date of current version September 22, 2021.

Digital Object Identifier 10.1109/ACCESS.2021.3112207

Adaptive Model-Mediated Teleoperation for Tasks Interacting With Uncertain Environment

CHEONGJUN KIM AND DOO YONG LEE, (Senior Member, IEEE)
Department of Mechanical Engineering, Korea Advanced Institute of Science and Technology, Daejeon 34141, South Korea

Corresponding author: Doo Yong Lee (leedy@kaist.ac.kr)

This work was supported in part by the National Research Foundation of Korea (NRF) grant funded by the Korean Government [Ministry of Science and ICT (MSIT)] under Grant 1711111113, and in part by Brain Korea 21 Plus Program in 2021.

This work involved human subjects or animals in its research. Approval of all ethical and experimental procedures and protocols was granted by the Institutional Review Board, Korea Advanced Institute of Science and Technology.

ABSTRACT Model-mediated teleoperation (MMT) employs an environment model at the master side to compute feedback output to the master at a faster rate. This approach improves system stability in the presence of time delay. MMT, however, does not generally perform well if the employed model is not accurate. The model mismatch is unavoidable when the environment is unknown in advance or varies. This paper proposes MMT employing an adaptive model. The proposed method adaptively moves the reference point of the employed model, whereas the previous MMTs used reference points fixed to the surface of objects in the environment. This can make system stability independent of the time delay. Experiments show that the proposed method improves stability compared to the previous MMTs when there are model mismatches. User studies are conducted to compare the operator's performance in two tasks, control of force exerted to objects in the environment, and discrimination of object stiffness. The result shows that the error in the forces applied to objects in the environment significantly decreases in the proposed method. Errors in forces rendered to the master are also improved by at least 20.2%. The experiment result also shows that subjects can discriminate up to 40.9% smaller differences in the stiffness than the previous MMT under the same time delay.

INDEX TERMS Haptics, teleoperation, stability, time delay.

I. INTRODUCTION

Bilateral teleoperation with haptic feedback has often been investigated for two practical tasks. The first is to control forces applied to objects. For example, robotic surgery often requires knot-tying after suturing [1]. Too much pulling force on the suturing string can break the fine suture or damage the soft tissue. The knot cannot be held firmly if the pulling force is too weak. Haptic feedback can also be used for handling fragile objects such as soft tissues [2] and explosive ordnances [3]. The second is to discriminate stiffness of objects. For example, a surgeon can distinguish normal healthy tissues from indurated tissues through haptic sensation [4]. The surgeon can also estimate the boundaries of the abnormal tissue. This paper aims to improve the performance of these two teleoperation tasks.

The associate editor coordinating the review of this manuscript and approving it for publication was Nasim Ullah.

Time delay between the master and the slave is one of the principal causes of instability in bilateral teleoperation [5]. A typical approach to maintain stability is to use adaptive dampers [6]–[9]. Software dampers are added to the master and slave controllers. Energy generated due to time delay is monitored and dissipated by the dampers. The operator in this approach, however, cannot predict the timing and magnitude of the time-varying damping force. Previous research reports experimental results showing that the unpredictable forces can disturb the operators [10]. Dyck *et al.* also show that the unpredictable forces can make the human operator effectively active and destabilize the system [11]. A teleoperation method not causing unpredictable force jumps to the operator, therefore, is desired.

Model-mediated teleoperation (MMT) [12], [13] improves system stability without using adaptive dampers. The master device's output to the human operator is computed by using a predefined force model describing the environment.

This work is licensed under a Creative Commons Attribution 4.0 License. For more information, see https://creativecommons.org/licenses/by/4.0/

Model parameters are estimated in real-time at the slave side and transmitted to the master side. Since the master output can be updated faster in the master's local loop, the time lag between the operator's input and the master's output to the user can be minimized. System stability, therefore, can be maintained regardless of the time delay between the master and the slave. This model-based force rendering to the operator can be physically reasonable in contrast to the approaches that physically unreasonably adjust or limit the master output to maintain system stability. Previous research reports a user study showing that MMT improves the success rate of the task controlling forces exerted to objects in the presence of time delay [14]. Tzafestas and Velanas also show that the operator can discriminate smaller stiffness differences using MMT than directly rendering the environment force to the master [15].

MMT, however, deteriorates when the predefined model is not accurate. Parameters estimated in real-time at the slave side may not converge continuously. The continuously changing parameter can be transmitted to the master side with time delay, causing lag between the input and the output to the master. Experimental result by Willaert *et al.* shows that the system is destabilized when the MMT using a linear stiffness model interacts with a nonlinear object [16]. Xu *et al.* show that an increase in the model stiffness generates energy and destabilizes the system [17]. They add an adaptive damper to dissipate the surplus energy. This approach, however, may cause unpredictable force jumps similar to other previous adaptive-damper-based methods. The previous MMT approaches may not be suitable when the environment impedance is unknown in advance or varies so that the model accuracy cannot be guaranteed.

Early MMTs use a model whose parameters are fixed to preset values [18]–[20]. This approach is utilized when the environment impedance is known in advance and static, such as rigid environment [21], [22]. The MMTs have been further developed to estimate the model parameters in real-time at the slave side to preserve the model accuracy. Various models have been also applied, such as linear spring model [16], [23]–[25], linear spring-damper model [26], linear mass-spring-damper model [27]–[29], linear spring with Coulomb friction [30], [31]. Hunt-Crossley model, a widely used nonlinear viscoelastic model, is also employed with MMT [32]. Deng *et al.* utilize a gradient boosting algorithm, a machine learning technique, to obtain a prediction model for the environment force in MMT [33]. They report that the gradient-boosting-based prediction is trained more accurately and faster than the Hunt-Crossley model. This approach, however, requires a training process prior to the actual operation. Chen *et al.* propose a teleoperation method to robustly control nonlinear manipulators [34], [35]. They employ an approach similar to MMT to avoid instability due to time delay. The master renders force feedback using the parameters transmitted from the slave side, and a radial basis function neural network is applied to model the reactive force of the environment.

Model jumps occur when the estimated parameters change abruptly, and in turn cause jumps in the master force. These abrupt and unpredictable changes can cause unintended move of the operator. An intuitive method to alleviate the model jump is limiting the change rate of the master force. Researches [16], [26] apply a proxy-based haptic rendering [36] to MMT. The velocity of the proxy is limited to make the master force change gradually without abrupt jumps. Song *et al.* propose a method limiting the force magnitude that can change during one sample time [37]. These methods, however, have differences between the forces rendered to the operator and the applied to objects in the environment, which can degrade task performance in control of force and discrimination of stiffness. There is a control-based approach [38] focusing on the model jump occurring when the slave contacts the environment.

This paper focuses on the stability problem in MMT. The problem is caused by energy generation due to the changing stiffness in the force model. The damping element in the model rather dissipates energy and tends to stabilize the system. The problem occurs even when the master and slave's local controllers and the model parameter estimation are stable and accurate. This paper proposes an MMT method which can solve the stability problem without adjusting the stiffness rendered to the operator, in contrast to the previous MMTs that adjust the rendered stiffness to stabilize the system.

Main idea is adaptively setting the reference point of the stiffness element responding to the stiffness update of the model. The reference point is moved so that the stiffness update cannot change the model's force output. This allows the master's state to be affected only by the operator's force input so that the system stability becomes independent of time delay regardless of the model accuracy. The adaptively moving spring approximates the environment force as a piecewise linear function. The approximation error is compensated by force control in the slave while interacting with the environment.

II. PRELIMINARY

This paper addresses the circumstances that the slave robot is palpating and touching the objects in the environment. This situation frequently occurs in many applications such as remote master-slave surgery and virtual simulation. The object in the environment is assumed to be soft and deformable. The scope of this paper does not cover the cases where the target object's position or topology changes. It is assumed that the object does not move during the palpation and indentation by the slave robot.

The interaction force, denoted as environment force in this paper, between the slave robot and the environment is mainly caused by the reaction force by the deformed object. The ''environment model'' in this paper indicates the relationship between the object's deformation and the reaction force. The environment model is used to compute the haptic feedback force rendered to the master device in MMT. The force

model's parameters are updated periodically to the value computed at the slave side.

This paper addresses the instability problem caused by the mismatch between the force model used in MMT and the actual environment model. The problem occurs even when the local controllers of the master device and the slave robot provide accurate and stable tracking. The term "uncertain environment" in this paper means that the actual environment force model is unknown, so that the MMT system cannot use accurately matched force models. Please note that the method proposed in this paper can be applied to other models, although this paper focuses on the linear stiffness model.

Since the focus of this paper is the master-slave haptic controller, the experiment setup employs the built-in local nonlinear controllers provided by the manufacturer of the manipulator used in the experiments as explained in Section V. The nonlinearity is taken care of by the built-in local controller that is not the scope of this paper. This paper focuses on solving the stability problem caused by the model mismatch in MMT method for master-slave haptic control, not on improving the performance of the manipulator's local controller. Please note that any kind of local controller can be used together with the model-update method proposed in this paper. The system implemented for the experiments in the paper is an example.

III. ADAPTIVE MODEL-MEDIATED METHOD

The master device in model-mediated teleoperation interacts with a model instead of actual environment. A simplified example is illustrated in Fig. 1 to show the improvement over the previous MMT. The example shows the situation where the master device interacts with a linear spring model whose stiffness changes. Since the changing stiffness causes the stability problem in the model, the force model is assumed to have stiffness element only in this example. The damping element rather dissipates energy and tends to stabilize the system.

The interaction force rendered to the user is computed as

$$f_{md} = -k_{md}\left(x_m - x^*_{md}\right), \tag{1}$$

where x_m and f_{md} denote the master position and the force computed by the model corresponding to the desired force of the master, respectively. The k_{md} and x^*_{md} indicate stiffness coefficient and the reference point of the model, respectively.

Fig. 2(a) and 2(b) show force profiles rendered for the cases Fig. 1(a) and 1(b). The model stiffness is updated from k_0 to k_1 when the master device reaches the position x_1. The f^-_{md} and f^+_{md} denote rendered output force from the model immediately before and after the update of model stiffness, respectively. The contact position between the slave and the actual environment is set to x^*_0.

Since the reference point of the model is fixed to the contact position x^*_0 in the previous MMTs, the output force changes discontinuously as the stiffness is updated as shown in Fig. 2(a). The force output rendered to the master device is instantly affected by the changes in the model parameters.

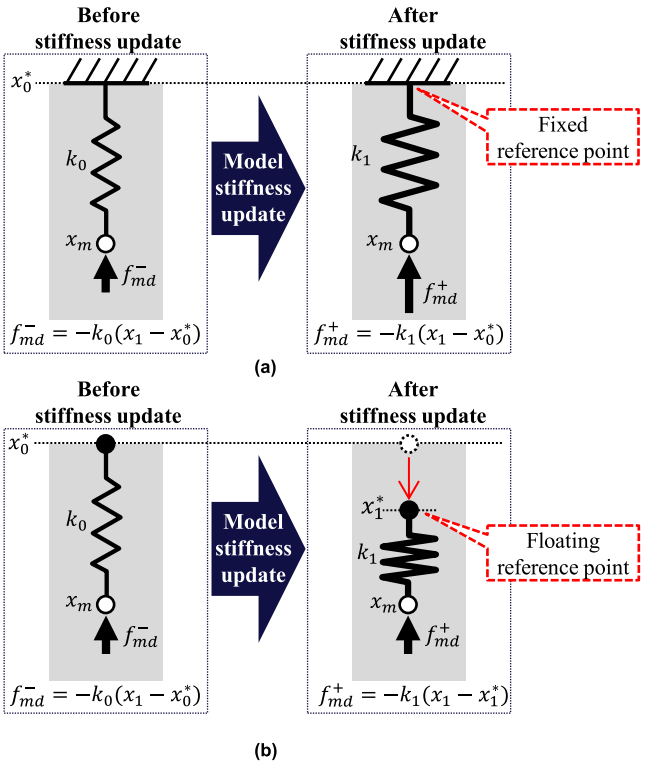

FIGURE 1. Examples where a master device interacts with a linear spring model, and the model stiffness is updated to a new value according to changing environment. (a) Previous MMTs use a fixed reference point for the employed models. (b) Proposed method uses a floating reference point, and adaptively sets the reference point responding to updates of model stiffness.

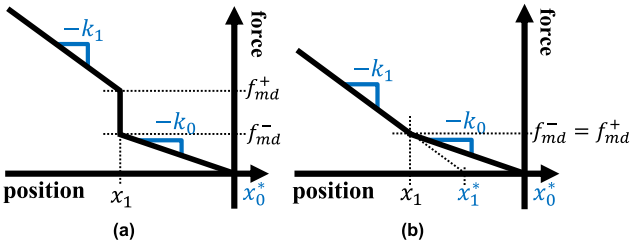

FIGURE 2. Force outputs rendered to the master device for the cases in Fig. 1 (a) Previous MMTs. (b) Proposed method.

The reference point of the model in the proposed method is, however, adjusted to a new value when the model stiffness is updated. The reference point is set to a position which allows the output force not to be changed abruptly by the stiffness update. The reference point moves from x^*_0 to x^*_1 as follows.

$$x^*_1 = x_1\left(\frac{k_1 - k_0}{k_1}\right). \tag{2}$$

Substituting (2) into the equation for f^+_{md} in Fig. 1(b), it can be shown that the forces before and after the stiffness update, f^-_{md} and f^+_{md}, are the same as shown in Fig. 2(b). Note that the movement of the reference point does not affect the stiffness rendered to the master device. This prevents discontinuous force changes under stiffness update, i.e. model jumps, without adjusting or limiting the stiffness rendered to the operator.

Previous MMTs limit the change rate of the master force to handle model jumps.

This approach also has an advantage in stability. The force rendered to the master device can be changed only by the operator's move since the stiffness update does not cause any change in the master force. The master's state is decoupled from the slave's state, and the master's command affects the slave's state. System stability becomes independent of the time delay between the master and the slave in contrast to the previous MMTs where the stability is significantly affected by the time delay when the model is not accurate.

The proposed method describes the environment force by a linear stiffness model whose stiffness and reference point vary. Environment force, therefore, is approximated by a piecewise-linear stiffness as shown in Fig. 2(b) as

$$\hat{f}_e = -\hat{k}_{e,k}\left(x_s - x_{s,k-1}\right) - \sum_{j=1}^{k-1} \hat{k}_{e,j}\left(x_{s,j} - x_{s,k-1}\right), \quad (3)$$

where $\hat{f}_e$ indicates the approximated force. The subscript k means the total number of linear segments consisting of the piecewise linear stiffness. The $\hat{k}_{e,k}$ and $x_{s,k-1}$ denote the stiffness coefficient and the starting position of the [k]th segment. The starting position of the first segment, $x_{s,0}$ corresponds to the contact position between the slave robot and the environment.

Fig. 3 shows an example of the force profile of an environment (solid line) and the corresponding rendered force approximated by the proposed method (dotted line). The x_s and f_e denote the slave position and the reactive force from the environment, respectively. The k_e indicates nonlinear stiffness of the environment. The x_s^* means the contact position and is assumed to be zero for this example.

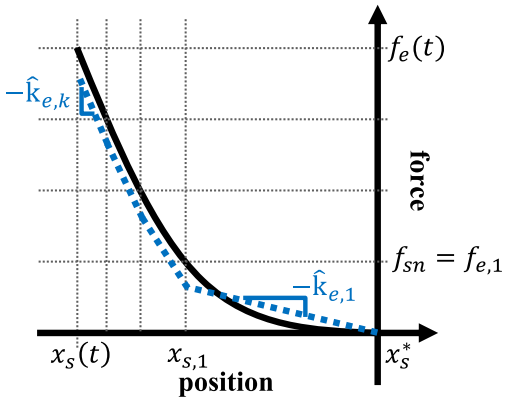

FIGURE 3. Force profiles of the actual environment (solid line) and the approximated by the proposed method (dotted line) when a slave interacts with a nonlinear stiffness object.

The stiffness of the linear spring in the proposed method is updated whenever the reactive force from the environment changes beyond a threshold f_{sn}. This is to attenuate the effect of measurement noise. The value of the threshold is determined considering the noise level.

The model stiffness is computed through linear fitting as

$$\hat{k}_{e,j} = -[\mathbf{x_j^T x_j}]^{-1}\mathbf{x_j^T f_j}, \quad (4)$$

where $\hat{k}_{e,j}$ denotes the [j]th stiffness coefficient. The $\mathbf{x_j}$ and $\mathbf{f_j}$ are the position and the force vectors, respectively, and are defined as

$$\mathbf{x_j} = \begin{bmatrix} x_{s,j} - x_{s,j-1} \\ \vdots \\ x_{s,j-1} - x_{s,j-1} \end{bmatrix}, \quad \mathbf{f_j} = \begin{bmatrix} f_{e,j} - f_{e,j-1} \\ \vdots \\ f_{e,j-1} - f_{e,j-1} \end{bmatrix} \quad (5)$$

where $x_{s,j}$ and $f_{e,j}$ denote the slave position and the environment force measured at the [j]th computation of stiffness. The initial values, $x_{s,0}$ and $f_{e,0}$, correspond to the position and the force when the slave contacts an object in the environment. Note that the difference between $f_{e,j}$ and $f_{e,j-1}$ is always equal to the threshold value f_{sn} since the stiffness computation is triggered each time the environment force changes beyond the threshold. The linear fitting (4) computes a stiffness coefficient which minimizes the squared error.

The computed stiffness is sent to the master side. The force to be rendered to the master, f_{md} is computed using the stiffness coefficient as

$$f_{md} = -k_{md,k}\left(x_m - x_{md,k}^*\right), \quad (6)$$

where

$$k_{md,k} = \hat{k}_{e,k}, \quad (7)$$

$$x_{md,k}^* = x_{m,k}^{th} - \frac{1}{k_{md,k}} \sum_{j=1}^{k-1} \left(k_{md,j}\left(x_{m,j+1}^{th} - x_{m,j}^{th}\right)\right). \quad (8)$$

The subscript k is the total number of the stiffness coefficients sent from the slave to the master. The $k_{md,k}$ and $x_{md,k}^*$ denote the [k]th stiffness coefficient and the reference point of the spring model at the time, respectively. The $\hat{k}_{e,k}$ is the [k]th stiffness coefficient sent from the slave, and $x_{m,j}^{th}$ indicates the master position at the moment when the [j]th stiffness is received.

The current stiffness of the model is set to the most recently received stiffness coefficient as in (7). The reference point of the model $x_{md,k}^*$ is also adjusted responding to the new stiffness as in (8). The reference point computed in (8) ensures that the force rendered to the master, f_{md} does not change abruptly due to the new stiffness coefficient. For example, when t^- and t^+ indicate the moments immediately before and after the new [k + 1]th stiffness coefficient is received, respectively, the master force before the reception is given by substituting (7) and (8) to (6) as

$$f_{md}(t^-) = -\hat{k}_{e,k}\left(x_m\left(t^-\right) - x_{m,k}^{th}\right) - \sum_{j=1}^{k-1}\left(\hat{k}_{e,j}\left(x_{m,j+1}^{th} - x_{m,j}^{th}\right)\right). \quad (9)$$

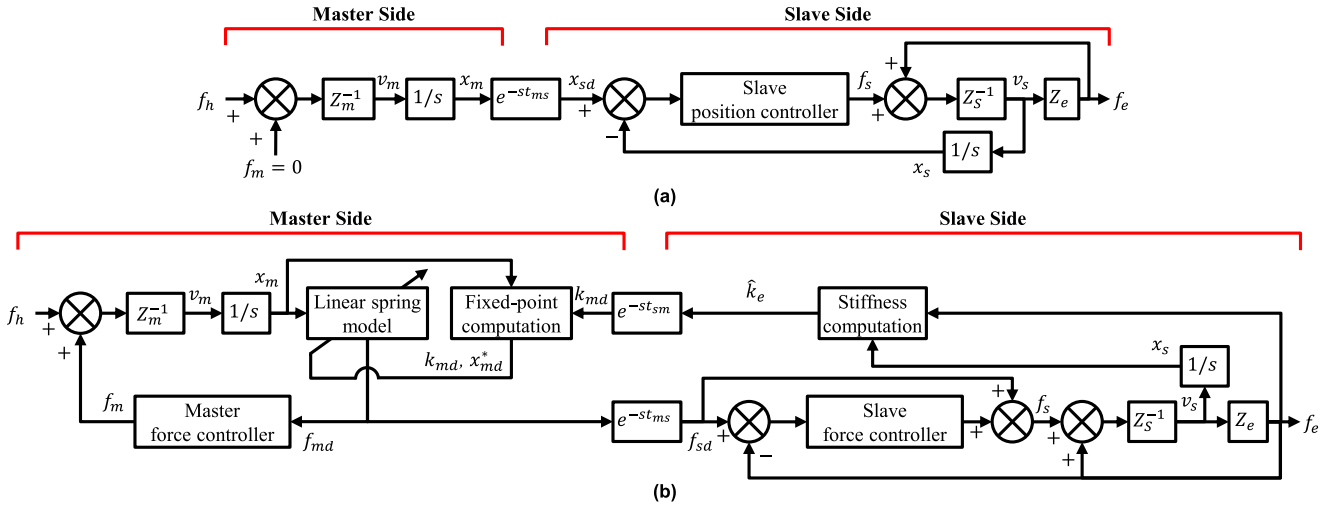

FIGURE 4. Two control schemes used in the proposed method. (a) position control mode. (b) force control mode.

After the [k + 1]th stiffness is received, the force becomes as

$$\begin{aligned} &f_{md}(t^+) \\ &= -\hat{k}_{e,k+1}\left(x_m\left(t^+\right) - x^{th}_{m,k+1}\right) - \hat{k}_{e,k}\left(x^{th}_{m,k+1} - x^{th}_{m,k}\right) \\ &\quad - \sum_{j=1}^{k-1}\left(\hat{k}_{e,j}\left(x^{th}_{m,j+1} - x^{th}_{m,j}\right)\right). \end{aligned} \tag{10}$$

Since $x^{th}_{m,k+1}$ is set to the master position measured when the [k + 1]th stiffness is applied, it is defined as

$$x^{th}_{m,k+1} = x_m\left(t^-\right). \tag{11}$$

By substituting (11) to (10), it can be shown that the master output is the same immediately before and after the stiffness update if the master does not move so that $x_m\left(t^+\right) = x_m\left(t^-\right)$. This means that the force rendered to the master is changed only when the operator moves the master device.

$$\begin{aligned} &f_{md}(t^+) \\ &= -\hat{k}_{e,k+1}\left(x_m\left(t^+\right) - x_m\left(t^-\right)\right) - \hat{k}_{e,k}\left(x_m\left(t^-\right) - x^{th}_{m,k}\right) \\ &\quad - \sum_{j=1}^{k-1}\left(\hat{k}_{e,j}\left(x^{th}_{m,j+1} - x^{th}_{m,j}\right)\right) \\ &= -\hat{k}_{e,k}\left(x_m\left(t^-\right) - x^{th}_{m,k}\right) - \sum_{j=1}^{k-1}\left(\hat{k}_{e,j}\left(x^{th}_{m,j+1} - x^{th}_{m,j}\right)\right) \\ &= f_{md}(t^-). \end{aligned} \tag{12}$$

When the master device is assumed to be a mass-damper system, the dynamics of the master device can be expressed as

$$f_h + f_m = m_m\ddot{x}_m + b_m\dot{x}_m, \tag{13}$$

where f_h and f_m denote the force applied by the human operator and the actuating force of the master device, respectively. The m_m and b_m indicate the effective mass and damping of the master device.

The force transmitted to the operator f_{to} corresponds to the negative value of the f_h as

$$f_{to} = -f_h = f_m - m_m\ddot{x}_m - b_m\dot{x}_m, \tag{14}$$

The desired force of the master device, f_{md} is rendered to the master as

$$f_m = f_{md}. \tag{15}$$

By substituting (6), (7) and (15) into (14),

$$f_{to} = \hat{k}_{e,k}\left(x_m - x^*_{md,k}\right) - m_m\ddot{x}_m - b_m\dot{x}_m. \tag{16}$$

The force transmitted to the operator consists of the interaction force computed by the model and the resistant force due to the impedance of the master device. Since the model's stiffness is periodically updated to the stiffness computed at the slave side, the operator can perceive the environment stiffness. Note that the resistant force due to the master's impedance is compensated in the experiment in Section V using the built-in controller provided by the device manufacturer.

The proposed method switches between position and force control modes depending on non-contact and contact states, respectively as shown in Fig. 4. The plants of the master device and the slave robot are noted as inverse impedances, Z_m^{-1} and Z_s^{-1}, respectively, in the block diagrams. The Z_m and Z_s denote the impedances of the master device and the slave robot, respectively. Position-force switching is widely used in the literature. During the contact state, the slave is controlled to exert a force commanded by the master as shown in Fig. 4(b). The force command corresponds to the desired force of the master, i.e. the force computed by the model.

Time delay can cause an error between the environment force f_e and the force command from the master f_{sd}. For example, the force command f_{sd} can be zero even when the

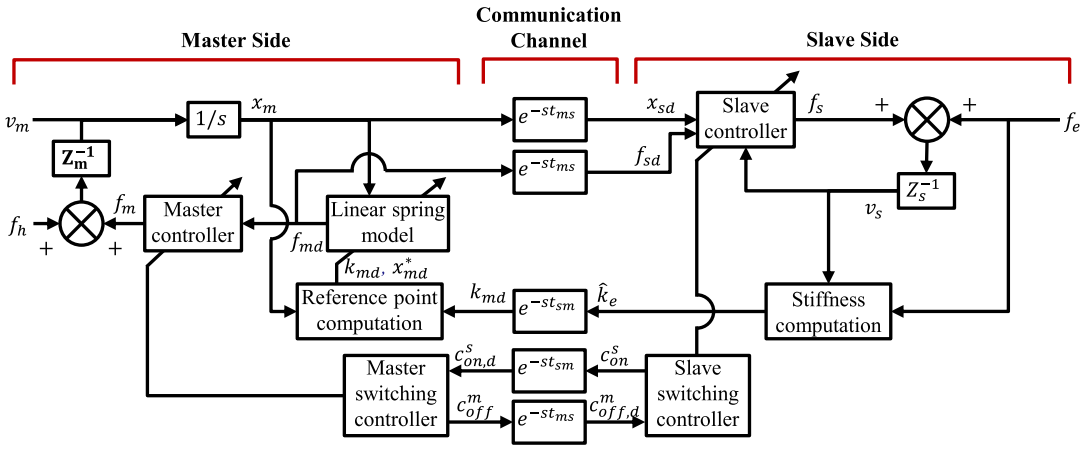

FIGURE 5. Overall control scheme of the proposed method.

slave has already contacted the environment. This can cause abrupt movement of the slave at the beginning of the force control mode. The proposed method, therefore, makes the slave hold its position after the first stiffness coefficient is computed at the slave side. At least one stiffness computation is required to begin force rendering at the master side. The slave waits for a command from the master, f_{sd} to reach the current environment force f_e. Position control is switched to force control mode only when the command f_{sd} becomes greater than or equal to the current environment force f_e so that $f_{sd}(t) \geq f_e(t)$. The force control mode begins only after the error between the command and the current environment force becomes zero.

During switching from force control to position control mode, the slave is made to hold its position after the environment force, f_e becomes smaller than the threshold f_{sn} so that $f_e(t) \leq f_{sn}$. The control mode is switched after the position command from the master x_{sd} becomes the same as the current slave position x_s. The slave controllers always starts with zero error in the proposed method. The switching does not affect system stability since it does not change the states of the master and the slave.

Fig. 5 shows the overall control architecture of the proposed method. The C^s_{on} and C^m_{off} are Boolean variables to switch the control modes.

IV. STABILITY OF THE PROPOSED METHOD

Since the master device renders no force during position control mode, the dynamics of the master device in (13) becomes as

$$f_h = m_m\ddot{x}_m + b_m\dot{x}_m, \tag{17}$$

This is a mass-damper system with a positive damping which is output-strictly passive [39], [40], so it is bounded-input-bounded-output (BIBO) stable. Therefore,

$$\lim_{t\to\infty} \sup |x_m(t)| < \infty \quad \text{for any bounded } f_h. \tag{18}$$

Since the position command to the slave x_{sd} is a delayed signal of the master position, it is also bounded with the master position x_m as

$$\lim_{t\to\infty} \sup |x_{sd}(t)| = \lim_{t\to\infty} \sup |x_m(t - t_{ms})| < \infty. \tag{19}$$

If the slave position controller guarantees BIBO stability,

$$\lim_{t\to\infty} \sup |x_s(t)| < \infty, \quad \text{for any bounded } x_{sd}. \tag{20}$$

From (13∼15), the following holds.

$$\lim_{t\to\infty} \sup |x_s(t)| < \infty, \quad \text{for any bounded } f_h, \tag{21}$$

if the slave position controller is BIBO stable. This indicates that the stability of the master-slave system is independent of time delay and depends only on the slave's position controller.

The master renders a force computed by the model during the force control mode so that $f_m = f_{md}$. The dynamics of the master devices is expressed as

$$f_h + f_{md} = m_m\ddot{x}_m + b_m\dot{x}_m. \tag{22}$$

Since the model's output forces are the same before and after the stiffness update in the proposed method as explained with (9∼12), the force model can be considered as a piecewise-linear spring whose stiffness k_{ps} varies according to the master's position as

$$f_{md}(t) = -k_{ps}(x_m(t))\left(x_m(t) - x^*_{ps}\right), \tag{23}$$

where x^*_{ps} denotes the reference point of the piecewise-linear spring. The x^*_{ps} is constant value corresponding to the master position when the stiffness coefficient is first sent from the slave.

Substituting (23) into (22), the master dynamics becomes as

$$f_h + k_{ps}x^{th}_{m,1} = m_m\ddot{x}_m + b_m\dot{x}_m + k_{ps}x_m. \tag{24}$$

This shows that the master's state is determined only by the operator's force input f_h in the proposed method.

Since the system is a forced mass-spring-damper system which is BIBO stable,

$$\lim_{t\to\infty} \sup |x_m(t)| < \infty \text{for any bounded } f_h. \quad (25)$$

Since k_{ps} and x^*_{ps} in (23) are finite values that depend on the environment, f_{md} is also bounded when x_m is bounded as

$$\lim_{t\to\infty} \sup |f_{md}(t)| < \infty \quad \text{for any bounded } x_m. \quad (26)$$

The force command to the slave f_{sd} is a delayed signal of the master force such that $f_{sd}(t) = f_{md}(t - t_{ms})$. Therefore, f_{sd} is also bounded with f_{md}, so

$$\lim_{t\to\infty} \sup |f_{sd}(t)| = \lim_{t\to\infty} \sup |f_{md}(t - t_{ms})| < \infty. \quad (27)$$

If the slave force controller guarantees BIBO stability,

$$\lim_{t\to\infty} \sup |x_s(t)| < \infty \quad \text{for any bounded } f_{sd}. \quad (28)$$

From (25∼28), the following holds.

$$\lim_{t\to\infty} \sup |x_s(t)| < \infty \quad \text{for any bounded } f_h, \quad (29)$$

if the slave force controller is BIBO stable. This implies that system stability is independent of any time delay and depends only on the local controller of the slave side during the force control mode as in the position control mode.

The proposed method, therefore, is applicable even when the environment model is not predefined accurately in contrast to the previous MMTs where model inaccuracy can cause instability in the presence of time delay.

V. EXPERIMENTS

A contact experiment is conducted to evaluate the proposed method. A master-slave system is formed using a commercial haptic device (Delta3 of Force Dimension) and a robot (LBR iiwa of KUKA Robotics) connected through TCP/IP communication as shown in Fig. 6. A force/torque sensor (Gamma of ATI Industrial Automation) is attached to the end-effector of the slave to measure the environment force.

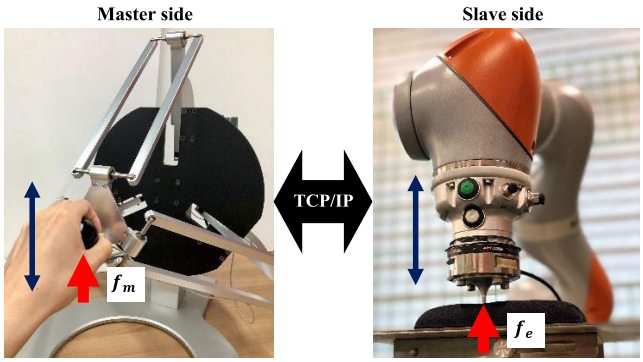

FIGURE 6. Setup for the contact experiment.

The master device is force-controlled at 4 kHz in open-loop mode using the embedded controller provided by the device manufacturer. It includes the compensator for the resistant force due to gravity, inertia, and damping of the device. The slave robot is also controlled by the built-in position controller in Robotics API provided by the manufacturer [41]. It is safely assumed that the built-in controller of the manufacturer provides asymptotically accurate velocity control so that $\lim_{t\to\infty} (\dot{x}_{sd}(t) - \dot{x}_s(t)) = 0$ where $\dot{x}_{sd}$ is the desired velocity of the slave robot. The built-in local controller provided by KUKA corresponds to the block in Fig. 7. The experiment results in Figs. 8 and 10 show that the built-in local position controller provided by KUKA stably controls the robot interacting with the target object made of compliant silicone. The control frequency is about 450 Hz. It is observed that the built-in position controller of the slave causes 30 ms time lag averagely between the position command and the robot position.

The force control of the slave is implemented based on the force controller reported in [42]. Fig. 7 shows the scheme of the force controller implemented for the experiment. The t_{fs} denotes the time when the force control mode starts. Environment stiffness is estimated in real-time to update the controller gain adaptively. It is noted that the estimated stiffness $\hat{k}_{fc}$ is different from the stiffness of the force model. The $\hat{k}_{fc}$ is used only for the force control of the slave robot, but not for the haptic rendering to the master device. The KUKA built-in position controller block corresponds to the slave position controller. The stiffness $\hat{k}_{fc}$ is estimated using a recursive least square algorithm with an exponential forgetting factor [43]. The forgetting factor is set to 0.1. The control gain k_f is set to 8 mm/Ns. When the position controller provides asymptotically accurate velocity control, the force controller provides asymptotically accurate regulation so that $\lim_{t\to\infty} (f_{sd} - f_e) = 0$. The derivation can be found in [42]. The experiment results in Fig.12 also show that the force control employing the built-in local position controller of the KUKA robot provides stable force control during the interaction.

The operator is requested to apply 4 N force to a silicone object and hold for at least 4 s. The reactive force over time is displayed to the operator in real-time.

Figs. 8 and 9 show the experiment results when a previous MMT is applied, mediated by a linear stiffness model. The slave is controlled to track the master position. The model stiffness is estimated using the recursive-least-square algorithm with an exponential forgetting factor [43], [44] that has been widely used to estimate time-varying parameters. The time delay between the master and the slave is virtually added. Figs. 8 and 9 are the results without and with a delay of 50 ms, respectively. The graphs in (a) show the positions and the forces of the master and the slave. The graphs in (b) are the force versus position. The graphs in (c) show the energy stored in the master. It is computed by integrating the force multiplied by the velocity of the master over time as

$$E_m(t) = \int_0^t -f_m(\tau) v_m(\tau) d\tau. \quad (30)$$

The graphs in (d) show the stiffness coefficient estimated at the slave side, and its initial value is set to 0.2 N/mm in the experiment.

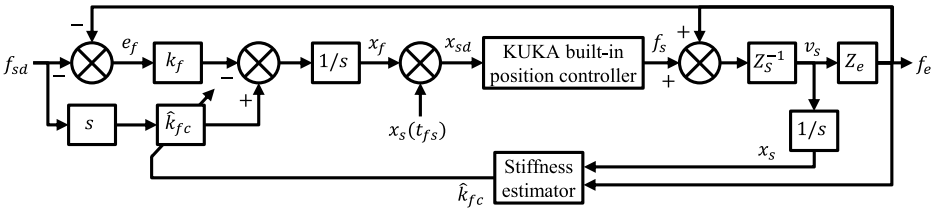

FIGURE 7. Architecture of the slave local force controller implemented for the contact experiment.

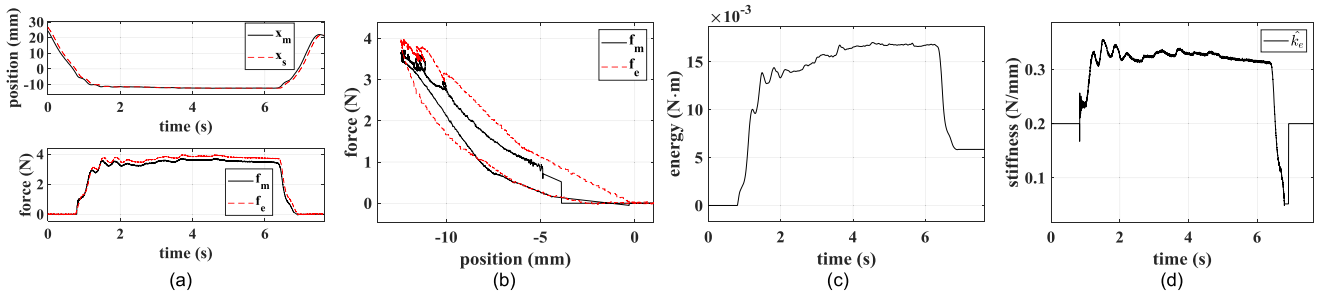

FIGURE 8. Experiment results of a previous MMT without time delay. (a) force and position over time (b) force versus position (c) energy (d) estimated stiffness.

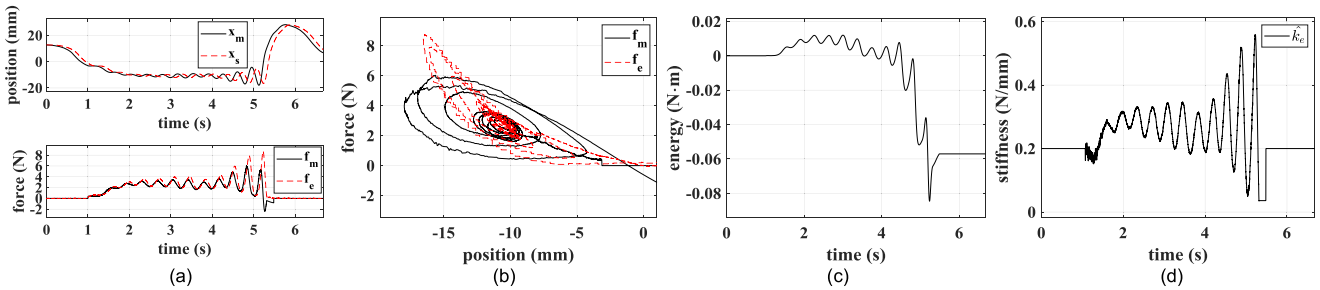

FIGURE 9. Experiment results of the previous MMT with time delay of 50 ms. (a) force and position over time (b) force versus position (c) energy (d) estimated stiffness.

The force profiles in (b) show that the environment has nonlinear impedance so that model mismatch occurs. The operator could keep the force as intended during the experiment when there is no additional time delay. But the task could not be accomplished when time delay is added. It was observed that the estimated stiffness changes continuously without converging due to the model mismatch. The graph in Fig. 9(b) shows that the continuously changing stiffness distorts the force profile of the master as a loop shape which rotates clockwise.

This shows that energy is repeatedly generated in the master so that the system becomes unstable. Fig. 9(c) shows that the energy storage decreases continuously during the interaction, which means energy generation. The instability causes more than 8 N, 119.9% increase, is applied to the environment.

Figs. 10 and 11 are the results of a previous MMT with the force-based model update algorithm (FMU) [37]. The algorithm limits the change rate of the force rendered to the master. The force-limiting gain is set to the same value used in [37]. Figs. 10 and 11 show the results without and with 50 ms time delay, respectively. The operator was able to maintain the force in both cases. The graphs in (c) show that energy is generated during the interaction in both cases as in the previous experiment. But the operator could stabilize the system since the master force changes slowly differently from the actual environment force.

The model update algorithm, however, causes additional force-rendering error as shown in (b). The force profiles rendered to the operator are distorted even when there is no time delay. The graph in Fig. 11(b) shows that negative impedance is rendered, physically unrealistic.

Figs. 12 and 13 show the results of the proposed method without and with the time delay, respectively. The threshold f_{sn} is set to 0.25 N considering the measurement noise. The operator was able to maintain the force under both delay conditions stably. The energy storage graphs in (c) remain positive during the interaction. This implies that energy is dissipated during the interaction, and system stability is maintained even in the presence of the time delay.

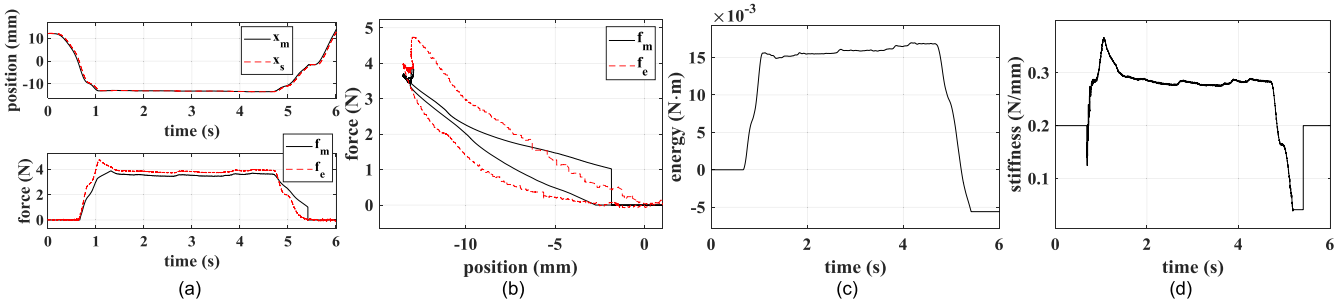

FIGURE 10. Experiment results of the previous MMT with model update, and no time delay. (a) force and position over time (b) force versus position (c) energy (d) estimated stiffness.

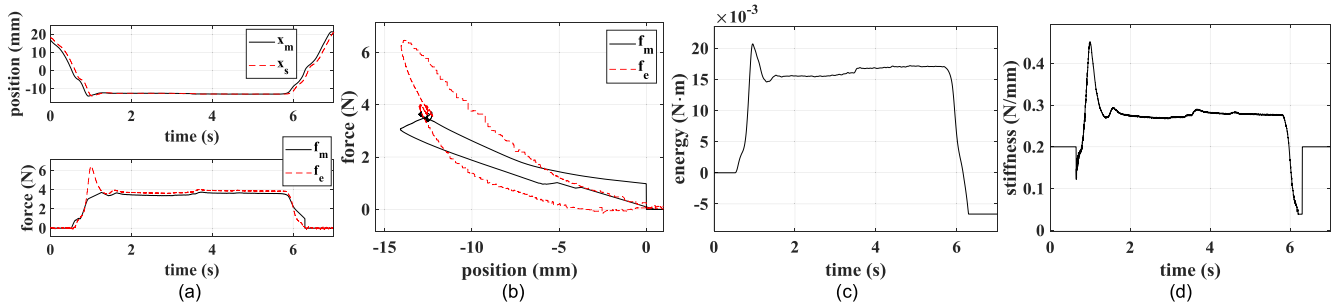

FIGURE 11. Experiment results of the previous MMT with model update, and 50 ms time delay. (a) force and position over time (b) force versus position (c) energy (d) estimated stiffness.

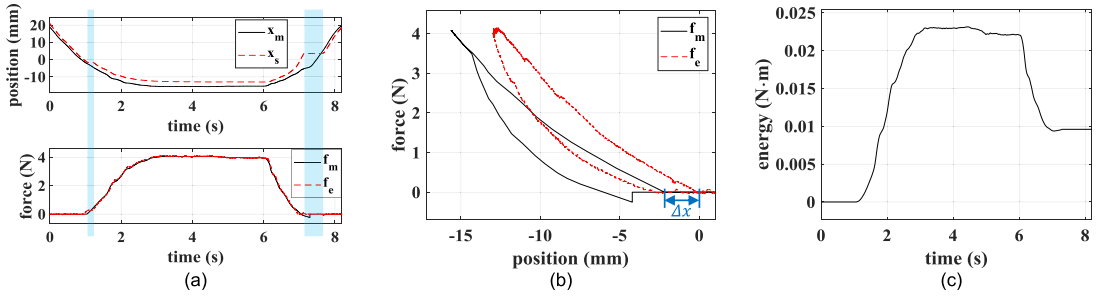

FIGURE 12. Experiment results of the proposed MMT without time delay. (a) force and position versus time (b) force versus position (c) energy versus time.

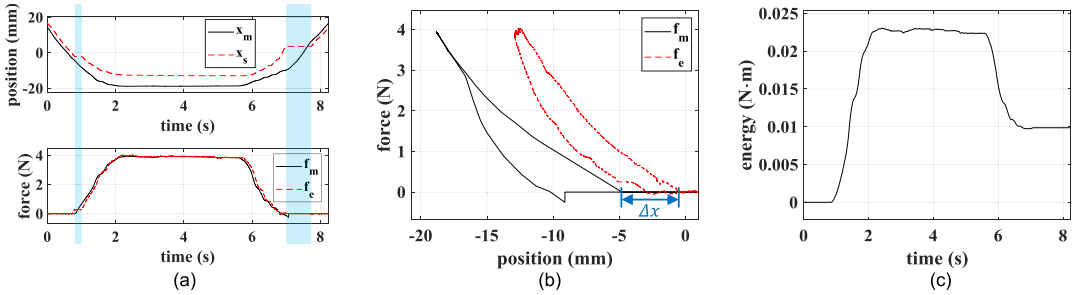

FIGURE 13. Experiment results of the proposed MMT with time delay of 50 ms. (a) force and position versus time (b) force versus position (c) energy versus time.

There is a difference between the master and the slave positions after the slave contacts the environment. The slave is controlled to hold its position immediately after the first stiffness computation. The slave starts to move again only after force command from the master exceeds the current environment force.

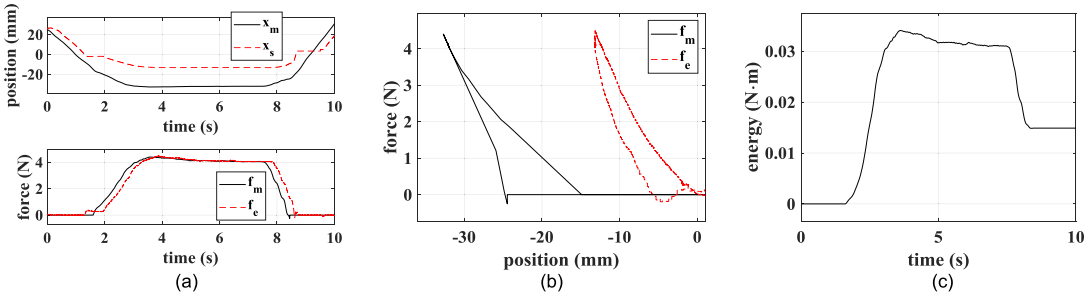

FIGURE 14. Experiment results of the proposed MMT with time delay of 250 ms. (a) force and position versus time (b) force versus position (c) energy versus time.

The master position where force rendering begins is different from the actual contact position of the slave. The position difference Δx is marked with arrows in the graphs in (b). The master starts force rendering only after the first stiffness coefficient is received from the slave. Note that the position where the master starts force rendering corresponds to $x_{m,1}^{th}$ in (8).

It is shown that the rendered forces in (b) have sharp turn-arounds. The proposed method computes a new stiffness coefficient whenever the environment force changes beyond a predefined threshold. The master renders constant stiffness until a new coefficient is sent from the slave. This sharp turn-around becomes longer as the time delay increases.

Fig. 14 shows the results of the proposed method when the one-way delay is set to 250 ms, four times the delay in the experiment in Fig. 13. It is observed that the tendency is similar to the results of 50 ms delay. System stability is maintained so that the operator is able to maintain the contact force stably. It is also shown that the larger delay causes the larger velocity difference between the master and the slave.

Since the environment force is described as a piecewise-linear spring in the proposed method, errors can exist between the actual stiffness and the model as

$$k_{md,k} = k_e\left(x_s\right) + \varepsilon_{n,k} + \varepsilon_{d,k} + \varepsilon_{t,k}. \tag{31}$$

where $\varepsilon_{n,k}$ and $\varepsilon_{d,k}$ denote the errors of the [k]th model stiffness due to the nonlinearity and the damping of the environment, respectively. The $\varepsilon_{t,k}$ means the error due to time delay. Since the computed stiffness is transmitted to the master side with delay, there is error between the two stiffness coefficients.

The effect of the error can be discussed by assuming the environment to be nonlinear viscoelasticity. When the stiffness and damping coefficients are assumed to be nonlinear functions of the slave position, the nonlinear environment force can be expressed as

$$f_e = -k_e\left(x_s\right)\left(x_s - x_s^*\right) - b_e\left(x_s\right)\dot{x}_s, \tag{32}$$

When the local force controller of the slave is assumed to have no tracking error,

$$f_e\left(t\right) = f_{md}\left(t - t_{ms}\right) = k_{md,k}\left(x_{md,k}^* - x_m\left(t - t_{ms}\right)\right). \tag{33}$$

By substituting (32) into (33),

$$-k_e\left(x_s\left(t\right)\right)\left(x_s\left(t\right) - x_s^*\right) - b_e\left(x_s\left(t\right)\right)\dot{x}_s\left(t\right) = k_{md,k}\left(x_{md,k}^* - x_m\left(t - t_{ms}\right)\right). \tag{34}$$

By differentiating both sides, the delayed master velocity can be derived as

$$\dot{x}_m\left(t - t_{ms}\right) = \left(\frac{\partial k_e}{\partial x_s}\left(x_s\left(t\right) - x_s^*\right)\dot{x}_s\left(t\right) + k_e\left(x_s\left(t\right)\right)\dot{x}_s\left(t\right) + \frac{\partial b_e}{\partial x_s}\dot{x}_s^2\left(t\right) + b_e\left(x_s\left(t\right)\right)\ddot{x}_s\left(t\right)\right) \Big/ \left(k_e\left(x_s\left(t\right)\right) + \varepsilon_{n,k} + \varepsilon_{d,k} + \varepsilon_{t,k}\right) \tag{35}$$

This implies that the stiffness error due to the nonlinearity and damping element of the environment, and time delay cause the velocity difference between the master and the slave. The velocity difference is shown in the experiments, but the user study in the following section shows this error does not significantly affect the performance of the two target tasks.

VI. USER STUDY

Experiments are carried out to test the two frequent goals of haptic feedback, force-applying and stiffness discrimination. Twenty-one subjects with an average age of 22.5 years volunteered for the experiments. All the subjects performed the same tasks of about 50 min. This user experiment is approved by the Institutional Review Board.

The same haptic device explained in Section V is connected to a 3D virtual environment constructed by an open-source library CHAI3D [45]. It is reasonably assumed that the local position and force control of the virtual slave robot have no error so that $x_s\left(t\right) = x_{sd}\left(t\right)$ and $f_e\left(t\right) = f_{sd}\left(t\right)$.

A. APPLYING FORCE

Fig. 15 shows the screen provided to subjects. The virtual environment consists of a box-shaped object, a vertical gauge, and a sphere which indicates the position of the slave end-effector. The box's width and the sphere's diameter are set to 200 mm and 5 mm, respectively. The vertical gauge shows the level of the force applied to the object. There is a marker in the middle of the gauge. The maker represents a target force. The subjects are asked to move the slave from the left edge

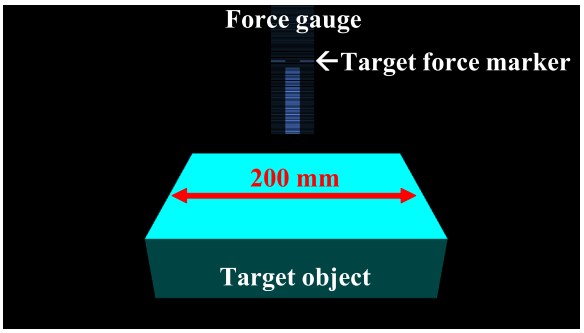

FIGURE 15. Screen provided to subjects during the force manipulation experiment.

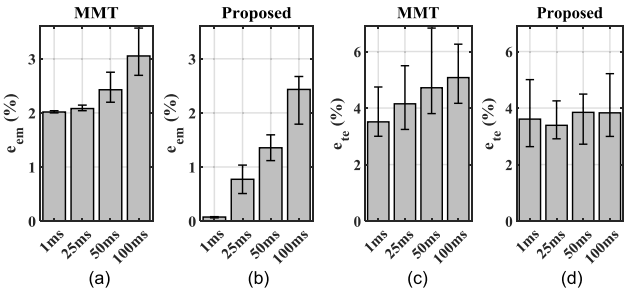

FIGURE 16. Medians and interquartile ranges measured at the force applying experiment. (a) e_{em} in the previous MMT (b) e_{em} in the proposed method (c) e_{te} in the previous MMT (d) e_{te} in the proposed method.

to the right edge of the box while applying the target force of 4 N.

The task is repeatedly carried out under four different time delay conditions, 1 ms, 25 ms, 50 ms, and 100 ms one way. The previous MMT with FMU and the proposed method are compared. The previous MMT without FMU was excluded from the experiment since a preliminary test showed poor stability.

The virtual object has nonlinear stiffness, and the MMTs are mediated by a linear stiffness model. Hence there is model mismatch. The environment force is given as

$$f_e = \begin{cases} k_e(x_s - x_s^*)^2, & x_s < x_s^* \\ 0, & x_s \geq x_s^*. \end{cases} \tag{36}$$

The stiffness coefficient k_e and the object surface position x_s^* are set to 0.025 N/mm^2 and 0 mm, respectively.

Two errors are measured as performance indices. First, the error between the environment and the master forces, e_{em} is given by

$$e_{em} = \sqrt{\frac{\sum_{i=i_l}^{i_r} \left(f_e\left(i\right) - f_m\left(i\right)\right)^2}{\sum_{i=i_l}^{i_r} \left(f_e\left(i\right)\right)^2}}, \tag{37}$$

where i_l and i_r denote the time steps when the slave passes through the left and the right edges of the object while pressing down the object. The error shows how accurately the environment force is rendered to the master. Second, the error between the target force of 4 N and the force applied to the environment, e_{te} is given as

$$e_{te} = \sqrt{\frac{\sum_{i=i_l}^{i_r} \left(f_{\text{target}} - f_e\left(i\right)\right)^2}{\sum_{i=i_l}^{i_r} \left(f_{\text{target}}\right)^2}}. \tag{38}$$

This indicates how accurately the operator can apply the requested force to the object.

Fig. 16 shows the experiment results. The data normality of each group is verified using Kolmogorov-Smirnov test. It is observed that e_{em} measured using MMT with FMU shows distribution significantly different from normal distribution under the 1 ms time delay condition, W = 0.3685, p = 0.0046. The results, therefore, are analyzed using Wilcoxon signed-rank test and Spearman correlation coefficient which are non-parametric tests.

Tables 1 and 2 show the results of Wilcoxon signed-rank test between the two control schemes. It is observed that the p-values for e_{em} are less than 0.05 under all the conditions of time delay. This means that the force-rendering error in the proposed method is significantly less than that in MMT regardless of the time delay. FMU, which limits the force change rate in the master, causes larger errors in force-rendering. In the case of e_{te}, all the p-values are less than 0.05 except when the delay is 1 ms. It can be interpreted as the error in force applying using the proposed method is significantly less than that in the previous MMT when the time delay is greater than 25 ms.

TABLE 1. Wilcoxon signed-rank test result of e_{em}.

Time delay (ms)	P-value	Signed-rank
1	9.537e-07	231
25	9.537e-07	231
50	9.537e-07	231
100	9.537e-07	226

TABLE 2. Wilcoxon signed-rank test result of e_{te}.

Time delay (ms)	P-value	Signed-rank
1	0.6578	129
25	0.0049	194
50	4.101e-05	221
100	0.0005	209

Tables 3 and 4 show Spearman correlation coefficients between the time delay and the e_{em} and e_{te}, respectively. The p-values confirm that e_{em} is significantly correlated with the time delay in both the previous MMT and the

TABLE 3. Spearman correlation between e_{em} and time delay.

	MMT w/ FMU	Proposed method
Rho	0.8563	0.9073
P-value	2.991e-25	1.371e-32

TABLE 4. Spearman correlation between e_{te} and time delay.

	MMT w/ FMU	Proposed method
Rho	0.3702	0.4787
P-value	0.0005	0.6655

proposed method. In the case of e_{te}, however, only the p-value in MMT is less than 0.05, which means a significant correlation between e_{te} and the time delay. Significant correlations are not observed in the proposed method. This implies that the capacity of applying accurate force is not significantly degraded by the increasing time delay when the proposed method is used. It can be expected that the gap in the force-controlling accuracy between the previous and the proposed methods will increase as the time delay increases.

B. STIFFNESS DISCRIMINATION

Stiffness discrimination is tested by measuring just-noticeable difference (JND) which indicates the minimum difference that a person can perceive. This experiment measures JND using the weighted 1up-4down method [46], [47]. Two objects are presented to subjects as shown in Fig. 17. The subjects are asked to choose a stiffer object. The stiffness difference between the two objects changes after each choice, and the task is repeated. Stiffness difference increases if the subject's choice is wrong and decreases if the answers are correct four times consecutively. The difference, as a result, converges to the value where the probabilities of the step-up and step-down become equal as the trials are repeated.

The ratio of the up and the down step sizes is set to 0.8415, following the guideline in [47]. One of the two objects is assigned reference stiffness, and the other is set to comparison stiffness. The reference stiffness is constant, and the comparison stiffness varies depending on the determined stiffness difference. The stiffness allocation changes randomly after each choice. The experiment is terminated when the stiffness difference changes its direction ten times. Fig. 18 shows stiffness differences collected during an experiment. The stiffness difference, initially, is set to decrease even if the choice is correct only once for quick approach to the convergence level. Four consecutively correct answers are required after the first incorrect answer occurs. The dotted circles in Fig. 18 indicate the reversal points where the up and down directions change. JND is computed by averaging the stiffness differences at the reversal points excluding the first reversal point as

$$\log(JND) = \sum_{i=2}^{10} \log(m_i)/9, \tag{39}$$

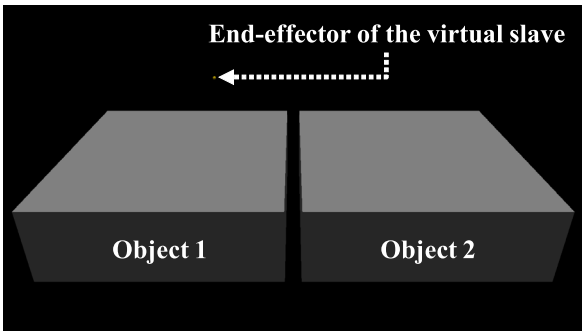

FIGURE 17. Screen provided to subjects during the stiffness discrimination experiment.

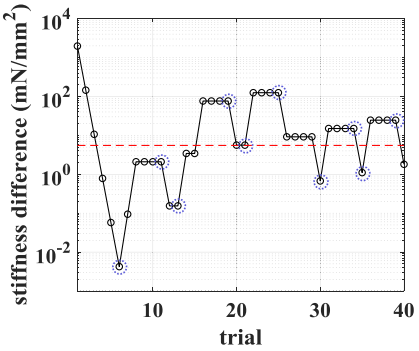

FIGURE 18. Change of the stiffness difference in the JND measurement.

TABLE 5. Wilcoxon signed-rank test between the JNDs measured in the two control schemes.

Time delay (ms)	P-value	Signed-Rank
1	0.0958	164
100	0.0142	46

where m_i denotes the stiffness difference at the i-th reversal point.

The objects have nonlinear stiffness as in (27). The reference stiffness and the initial value of the comparison stiffness are set to 0.025 N/mm^2 and 2 N/mm^2, respectively. The initial stiffness difference is 1.975 N/mm^2. If the stiffness difference exceeds 100 N/mm^2 by repeated wrong choices, the experiment is terminated before ten reversals. This means that the subject is unable to discriminate the large difference, and the JND is recorded as 100 N/mm^2 in this case. The experiment is conducted under the two different time delay conditions, 1 ms, and 100 ms, one way, using the previous MMT with FMU and the proposed method.

Fig. 19 shows the median and the interquartile range of the measured JNDs. Table 5 is the result of Wilcoxon signed-rank test between the JNDs measured using the two control schemes. A p-value less than 0.05 is observed when the delay is 100 ms, which implies that the JND decreases significantly in the proposed method. Table 6 shows the Spearman correlation between JND and time delay. The p-values in both cases are less than 0.05. The results of

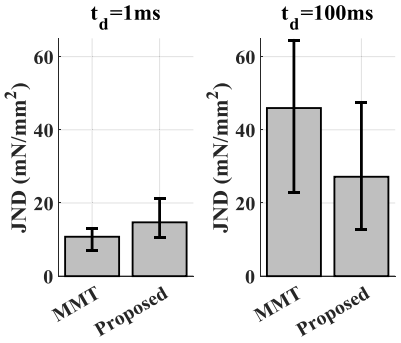

FIGURE 19. Medians and interquartile ranges of the measured JNDs.

TABLE 6. Spearman correlation coefficient between JND and time delay.

	MMT w/ FMU	Proposed method
Rho	0.7096	0.3223
P-value	1.431e-07	0.0374

the two tests confirm that the operator's capacity to discriminate the stiffness decreases significantly with the time delay in both control schemes. But the proposed method significantly outperforms the previous method when the time delay is 100 ms. The rho value of the proposed method is less than the previous MMT. This means that the JND increases more with the time delay in the previous MMT compared to the proposed method. It can be expected that the gap between the previous and the proposed methods will become larger as the time delay increases.

VII. CONCLUSION

This paper proposes an enhanced MMT method. The adaptive reference point makes parameter updates of the model does not cause any change in the force rendered to the master. The master's state is changed only when the operator moves the master. Stability of the master-slave control system becomes independent of the time delay between the master and the slave in contrast to the previous MMTs where the system can become unstable by the time delay when the employed model is not accurate.

A contact experiment shows that the proposed method maintains system stability even under the delay that the previous method becomes unstable. The force output rendered to the master device is less distorted in the proposed method than that in the previous MMT. Time delay causes physically unrealistic impedance in the previous method. The proposed method causes position differences between the master and the slave while interacting with the environment, instead of avoiding model jumps and system instability. The position difference makes the operator feel as if the contact position is lower than the actual environment position.

Results of the user study show that the position difference in the proposed method does not significantly degrade the operator's performance. The experiment verifies that the force-rendering accuracy is significantly improved in the proposed method under all delay conditions. The proposed method enhances the operator's ability to control the force applied to an object, and the improvement is significant when the delay is greater than or equal to 25 ms. The force-controlling ability is significantly degraded by the increasing time delay in the previous MMT, whereas no significant difference is observed in the proposed method. The stiffness discrimination experiment confirms that subjects are able to discriminate up to 40.9% smaller difference in the proposed method than that in the previous MMT under 100 ms delay.

Future work can be to extend MMT for the situations where the target object's position changes. Since MMT provides haptic feedback force to the operator through the environment force model, rapidly reflecting the object's changes to the model is necessary to extend MMT for the fast-changing scenario. The speed of the model update is affected by the time to estimate the model parameters at the slave side and the time to compute the force model. This implies that simpler models with fewer parameters would be advantageous to the faster estimation and update performance. The method proposed in this paper enables the MMT system to use a mismatched but simpler model.

REFERENCES

[1] N. Enayati, E. D. Momi, and G. Ferrigno, "Haptics in robot-assisted surgery: Challenges and benefits," *IEEE Rev. Biomed. Eng.*, vol. 9, pp. 49–65, 2016.
[2] X. Yin, S. Guo, H. Hirata, and H. Ishihara, "Design and experimental evaluation of a teleoperated haptic robot–assisted catheter operating system," *J. Intell. Mater. Syst. Struct.*, vol. 27, no. 1, pp. 3–16, Jan. 2016.
[3] S. Nahavandi, J. Mullins, M. Fielding, H. Abdi, and Z. Najdovski, "Countering improvised explosive devices through a multi-point haptic teleoperation system," in *Proc. IEEE Int. Symp. Syst. Eng.*, Rome, Italy, Sep. 2015, pp. 190–197.
[4] S. Chew, A. Wattiez, and L. Chomicki, *Basic Laparoscopic Techniques and Advanced Endoscopic Suturing: A Practical Guidebook*. Singapore: Singapore Univ. Press, 2000.
[5] R. Anderson and M. W. Spong, "Bilateral control of teleoperators with time delay," *IEEE Trans. Autom. Control*, vol. 34, no. 5, pp. 494–501, May 1989.
[6] P. F. Hokayem and M. W. Spong, "Bilateral teleoperation: An historical survey," *Automatica*, vol. 42, no. 12, pp. 2035–2057, Dec. 2006.
[7] T. A. Varkonyi, I. J. Rudas, P. Pausits, and T. Haidegger, "Survey on the control of time delay teleoperation systems," in *Proc. IEEE 18th Int. Conf. Intell. Eng. Syst.*, Jul. 2014, pp. 89–94.
[8] R. Muradore and P. Fiorini, "A review of bilateral teleoperation algorithms," *Acta Polytech. Hung.*, vol. 13, no. 1, pp. 191–208, 2016.
[9] J.-H. Ryu, J. Artigas, and C. Preusche, "A passive bilateral control scheme for a teleoperator with time-varying communication delay," *Mechatronics*, vol. 20, no. 7, pp. 812–823, 2010.
[10] X. Xu, Q. Liu, and E. Steinbach, "Toward QoE-driven dynamic control scheme switching for time-delayed teleoperation systems: A dedicated case study," in *Proc. IEEE Int. Symp. Haptic, Audio Vis. Environ. Games*, Abu Dhabi, United Arab Emirates, Oct. 2017, pp. 1–6.
[11] M. Dyck, A. Jazayeri, and M. Tavakoli, "Is the human operator in a teleoperation system passive?" in *Proc. IEEE World Haptics*, Daejeon, South Korea, Apr. 2013, pp. 683–688.
[12] X. Xu, B. Cizmeci, C. Schuwerk, and E. Steinbach, "Model-mediated teleoperation: Toward stable and transparent teleoperation systems," *IEEE Access*, vol. 4, pp. 425–449, 2016.
[13] A. A. Ateya, A. Muthanna, A. Vybornova, I. Gudkova, Y. Gaidamaka, A. Abuarqoub, A. D. Algarni, and A. Koucheryavy, "Model mediation to overcome light limitations—Toward a secure tactile internet system," *J. Sens. Actuators Netw.*, vol. 8, no. 1, p. 6, Jan. 2019.

[14] P. Mitra and G. Niemeyer, "Mediating time delayed teleoperation with user suggested models: Implications and comparative study," in *Proc. IEEE Symp. Haptic Interfaces Virtual Environ. Teleoperator Syst.*, Reno, NV, USA, Mar. 2008, pp. 343–350.

[15] C. Tzafestas and S. Velanas, "Telehaptic perception of delayed stiffness using adaptive impedance control: Experimental psychophysical analysis," *Presence Teleoper. Virtual Environ.*, vol. 22, no. 4, pp. 323–344, 2013.

[16] B. Willaert, H. Van Brussel, and G. Niemeyer, "Stability of model-mediated teleoperation: Discussion and experiments," in *Proc. Int. Conf. Hum. Haptic Sens. Touch Enabled Comput. Appl.*, Berlin, Germany, 2012, pp. 625–636.

[17] X. Xu, C. Schuwerk, and E. Steinbach, "Passivity-based model updating for model-mediated teleoperation," in *Proc. IEEE Int. Conf. Multimedia Expo Workshops (ICMEW)*, Turin, Italy, Jun. 2015, pp. 1–6.

[18] F. T. Buzan and T. B. Sheridan, "A model-based predictive operator aid for telemanipulators with time delay," in *Proc. Int. Conf. Syst., Man Cybern.*, Cambridge, MA, USA, Nov. 1989, pp. 138–143.

[19] T. Kotoku, "A predictive display with force feedback and its application to remote manipulation system with transmission time delay," in *Proc. IEEE/RSJ Int. Conf. Intell. Robots Syst.*, Raleigh, NC, USA, vol. 1, Jul. 1992, pp. 239–246.

[20] W.-K. Yoon, T. Goshozono, H. Kawabe, M. Kinami, Y. Tsumaki, M. Uchiyama, M. Oda, and T. Doi, "Model-based space robot teleoperation of ETS-VII manipulator," *IEEE Trans. Robot. Autom.*, vol. 20, no. 3, pp. 602–612, Jun. 2004.

[21] D. Valenzuela-Urrutia, R. Muñoz-Riffo, and J. Ruiz-del-Solar, "Virtual reality-based time-delayed haptic teleoperation using point cloud data," *J. Intell. Robot. Syst.*, vol. 96, nos. 3–4, pp. 387–400, Feb. 2019.

[22] H. Beik-Mohammadi, M. Kerzel, B. Pleintinger, T. Hulin, P. Reisich, A. Schmidt, A. Pereira, S. Wermter, and N. Y. Lii, "Model mediated teleoperation with a hand-arm exoskeleton in long time delays using reinforcement learning," in *Proc. 29th IEEE Int. Conf. Robot Hum. Interact. Commun. (RO-MAN)*, Naples, Italy, Aug. 2020, pp. 713–720.

[23] C. Tzafestas, S. Velanas, and G. Fakiridis, "Adaptive impedance control in haptic teleoperation to improve transparency under time-delay," in *Proc. IEEE Int. Conf. Robot. Autom.*, Pasadena, CA, USA, May 2008, pp. 212–219.

[24] X. Xu, J. Kammerl, R. Chaudhari, and E. Steinbach, "Hybrid signal-based and geometry-based prediction for haptic data reduction," in *Proc. IEEE Int. Workshop Haptic Audio Vis. Environ. Games*, Qinhuangdao, China, Oct. 2011, pp. 68–73.

[25] B. Willaert, J. Bohg, H. Van Brussel, and G. Niemeyer, "Towards multi-DOF model mediated teleoperation: Using vision to augment feedback," in *Proc. IEEE Int. Workshop Haptic Audio Vis. Environ. Games*, Munich, Germany, Oct. 2012, pp. 25–31.

[26] P. Mitra and G. Niemeyer, "Model-mediated telemanipulation," *Int. J. Robot. Res.*, vol. 27, no. 2, pp. 253–262, Feb. 2008.

[27] F. Mobasser and K. Hashtrudi-Zaad, "Stable impedance reflecting teleoperation with online collision prediction," in *Proc. IEEE/RSJ Int. Conf. Intell. Robots Syst.*, San Diego, CA, USA, Oct. 2007, pp. 476–482.

[28] H. Li and A. Song, "Virtual-environment modeling and correction for force-reflecting teleoperation with time delay," *IEEE Trans. Ind. Electron.*, vol. 54, no. 2, pp. 1227–1233, Apr. 2007.

[29] X. Xu, A. Song, D. Ni, H. Li, P. Xiong, and C. Zhu, "Visual-haptic aid teleoperation based on 3-D environment modeling and updating," *IEEE Trans. Ind. Electron.*, vol. 63, no. 10, pp. 6419–6428, Oct. 2016.

[30] X. Xu, B. Cizmeci, and E. Steinbach, "Point-cloud-based model-mediated teleoperation," in *Proc. IEEE Int. Symp. Haptic Audio Vis. Environ. Games*, Istanbul, Turkey, Oct. 2013, pp. 69–74.

[31] X. Xu, B. Cizmeci, A. Al-Nuaimi, and E. Steinbach, "Point cloud-based model-mediated teleoperation with dynamic and perception-based model updating," *IEEE Trans. Instrum. Meas.*, vol. 63, no. 11, pp. 2558–2569, May 2014.

[32] C. Liu, J. Guo, and P. Poignet, "Nonlinear model-mediated teleoperation for surgical applications under time variant communication delay," *IFAC-Papers Line*, vol. 51, no. 22, pp. 493–499, 2018.

[33] Q. Deng, T. Faghanimakrani, and A. H. Aghvami, "GBDT-based modules for force prediction in a model-mediated teleoperation system," in *Proc. 27th Int. Conf. Telecommun. (ICT)*, Bali, IN, USA, Oct. 2020, pp. 1–6.

[34] Z. Chen, F. Huang, W. Chen, J. Zhang, W. Sun, J. Chen, J. Gu, and S. Zhu, "RBFNN-based adaptive sliding mode control design for delayed nonlinear multilateral telerobotic system with cooperative manipulation," *IEEE Trans. Ind. Informat.*, vol. 16, no. 2, pp. 1236–1247, Feb. 2020.

[35] Z. Chen, F. Huang, W. Sun, J. Gu, and B. Yao, "RBF-neural-network-based adaptive robust control for nonlinear bilateral teleoperation manipulators with uncertainty and time delay," *IEEE/ASME Trans. Mechatronics*, vol. 25, no. 2, pp. 906–918, Apr. 2020.

[36] F. Ryden and H. J. Chizeck, "A proxy method for real-time 3-DOF haptic rendering of streaming point cloud data," *IEEE Trans. Haptics*, vol. 6, no. 3, pp. 257–267, Jul. 2013.

[37] J. Song, Y. Ding, Z. Shang, and J. Liang, "Model-mediated teleoperation with improved stability," *Int. J. Adv. Robotic Syst.*, vol. 15, no. 2, Mar. 2018, Art. no. 172988141876113.

[38] B. Yazdankhoo and B. Beigzadeh, "Increasing stability in model-mediated teleoperation approach by reducing model jump effect," *Scientia Iranica*, vol. 26, no. 1, pp. 3–14, 2019.

[39] S. Hirche and M. Buss, "Human-oriented control for haptic teleoperation," *Proc. IEEE*, vol. 100, no. 3, pp. 623–647, Mar. 2012.

[40] H. K. Khalil, "Passivity," in *Nonlinear Systems*, 3rd ed. Upper Saddle River, NJ, USA: Prentice-Hall, 2002, ch. 6, pp. 227–262.

[41] *com.kuka.robotics API (Ver. 1.15.2), KUKA AG*. [Online]. Available: http://www.com.kuka.robotics

[42] J. Roy and L. L. Whitcomb, "Adaptive force control of position/velocity controlled robots: Theory and experiment," *IEEE Trans. Robot. Autom.*, vol. 18, no. 2, pp. 121–137, Apr. 2002.

[43] A. Haddadi and K. Hashtrudi-Zaad, "Real-time identification of Hunt–Crossley dynamic models of contact environments," *IEEE Trans. Robot.*, vol. 28, no. 3, pp. 555–566, Jun. 2012.

[44] R. Schindeler and K. Hashtrudi-Zaad, "Online identification of environment Hunt–Crossley models using polynomial linearization," *IEEE Trans. Robot.*, vol. 34, no. 2, pp. 447–458, Apr. 2018.

[45] *CHAI3D. (3.2.0)*. Accessed: Feb. 15, 2021. [Online]. Available: https://www.chai3d.org/download/releases

[46] F. A. A. Kingdom and N. Prins, "Adaptive methods," in *Psychophysics: A Practical Introductions*, 2nd ed. Amsterdam, The Netherlands: Elsevier, 2016.

[47] M. A. Garcıa-Pérez, "Forced-choice staircases with fixed step sizes: Asymptotic and small-sample properties," *Vis. Res.*, vol. 38, no. 12, pp. 1861–1881, Jun. 1998.

CHEONGJUN KIM received the B.S. degree from the Department of Mechanical Engineering, Sungkyunkwan University, South Korea, in 2012, and the M.S. and Ph.D. degrees from the Department of Mechanical Engineering, Korea Advanced Institute of Science and Technology, South Korea, in 2014 and 2021, respectively. He is currently a Postdoctoral Researcher with Korea Advanced Institute of Science and Technology. His research interests include haptics, teleoperation, and medical robotics.

DOO YONG LEE (Senior Member, IEEE) received the B.S. degree from the Department of Control and Instrumentation Engineering, Seoul National University, South Korea, in 1985, and the M.S. and Ph.D. degrees from the Department of Electrical, Computer, and Systems Engineering, Rensselaer Polytechnic Institute, Troy, NY, USA, in 1987 and 1993, respectively. He was a Postdoctoral Research Associate with Rensselaer Polytechnic Institute, from 1993 to 1994. He joined the Department of Mechanical Engineering, Korea Advanced Institute of Science and Technology (KAIST), in 1994. He was the Director of Health Technology Infrastructure with Korea Health Industry Development Institute, from 2010 to 2012, and the Head of the Department of Mechanical Engineering, KAIST, from 2017 to 2021. He is currently the President of the Institute of Control, Robotics, and Systems. He is also the POSCO Endowed Chair Professor with KAIST. His research interests include robotics and simulation with medical applications, especially robotic medical devices, and high-fidelity interactive medical simulation with haptic interface for training and planning purposes. He is a member of the National Academy of Engineering of Korea. He received Korea Prime Minister's Commendation for technical contributions to the field, in 2018.